JOURNAL OF APPLIED ELECTROCHEMISTRY **27** (1997) 1232–1244

REVIEWS IN APPLIED ELECTROCHEMISTRY No. 48

Reaction and system modelling for Pb and PbO_2 electrodes

F. E. VARELA, E. N. CODARO, J. R. VILCHE*

Instituto de Investigaciones Fisicoquímicas Teóricas y Aplicadas (INIFTA), Facultad de Ciencias Exactas, Universidad Nacional de La Plata, Sucursal 4, C.C. 16, (1900) La Plata, Argentina

Received 6 January 1997; revised 17 March 1997

Reaction models for the metal dissolution, active–passive transition and passive layer electroreduction processes taking place during discharge/charge of the electrode active materials in the lead/sulphuric acid system are discussed. Reaction and system modelling can be evaluated on the base of results obtained from steady-state polarization, potentiostatic pulses, single (STPS) and repetitive (RTPS) triangular potential sweeps, modulated voltammetry, complex voltammetry combined with potentiostatic steps, and electrochemical impedance spectroscopy (EIS), using rotating ring Pb-disc Pb-electrode assemblies, as well as scanning electron microscopy (SEM). Data analysis derived from transient electrochemical techniques employing both parametric identification procedures, nonlinear fit routines and computer simulations has been interpreted in terms of appropriate nucleation and growth models for the formation of new phases, in which the characteristics and properties of the compounds generated on electrode surface exhibit a remarkable dependence on the corresponding operational potential.

Keywords: *lead/sulphuric acid system, lead electrooxidation, lead sulphate, lead monoxide, lead dioxide, nucleation and growth mechanisms*

1. Introduction

The first lead–acid cell was developed by Planté in 1859 [1]. As a consequence of his experiments with electrolytic polarization, Planté designed a battery to accumulate electric energy that consisted of spirally rolled lead leaves separated by rubber bands. This assemblage was then immersed in dilute sulphuric acid solution. This battery was presented to the French Academy of Sciences in 1860, where it excelled for the high currents that it could produce, higher than those of any other battery device existing at that time.

In 1882, Triber and Gladston proposed the 'double-sulphate theory' [2], which was initially strongly resisted, but is accepted today. This can be expressed through the following reaction:

$$PbO_2 + Pb + 2\,H_2SO_4 \underset{\text{charge}}{\overset{\text{discharge}}{\rightleftharpoons}} 2\,PbSO_4 + 2\,H_2O \quad (1)$$

The term 'double-sulphate' originates in the fact that lead sulphate is formed in both the negative and the positive plates during the discharge process. In the positive electrode, lead dioxide reacts with sulphuric acid to form lead sulphate and water,

$$PbO_2 + 4\,H^+ + SO_4^{2-} + 2\,e^- \xrightarrow{\text{discharge}} PbSO_4 + 2\,H_2O \quad (2)$$

while, in the negative electrode, metallic lead reacts with the sulphate ion to form lead sulphate,

$$Pb + SO_4^{2-} \xrightarrow{\text{discharge}} PbSO_4 + 2\,e^- \quad (3)$$

Understanding of the initial steps involved in the formation and reduction reaction of the films grown on lead in sulphuric acid solutions is very important in order to understand the elemental processes during battery operation. Study of the kinetics and mechanisms of the surface phenomena can be performed using potential-controlled perturbation techniques such as potential sweep methods combined with potentiostatic steps.

This work surveys studies concerning the processes of formation and reduction of the surface films on lead electrodes in the potential regions corresponding to the lead compounds produced on both the negative and the positive battery electrodes.

2. Lead (negative) electrode

2.1. *Anodic dissolution (discharge process) of lead electrodes*

Pb(II) ion solubility is generally low in aqueous solutions, and particularly in sulphuric acid solutions, because of the formation of $PbSO_4$. The amount of $PbSO_4$ in solution varies slightly with H_2SO_4 concentration, although in the range $0.06\,\text{M} \leq C_{H_2SO_4} \leq 11.5\,\text{M}$ the solubility remains close to $S_{PbSO_4} \approx 10^{-5}\,\text{M}$ [3]. Nevertheless, a narrow potential region in which lead dissolves freely has been identified [4–7]. Several researches have studied this process,

* Author to whom correspondence should be addressed.

0021-891X

but the governing mechanism is not completely established. Thus, although the Pb/Pb(II) charge transfer reaction has been interpreted as being completely reversible, and identified as the current limited by the diffusion of soluble Pb(II) species from the electrode surface [8], the process generally appears as controlled by a surface reaction involving adsorbed compounds, probably corresponding to Pb(I)-containing species. Thus, the experimental evidence has been interpreted in terms of consecutive charge transfer steps, in which the first, $Pb \rightarrow Pb(I)$ [7], as well as the second, $Pb(I) \rightarrow Pb(II)$ [9], has been considered rate determining.

Alternatively, Hampson *et al.* [5] considered the recombination of Pb(I) species on the electrode surface, giving a second adsorbed intermediate $(Pb(I))_2$. This mechanism can be expressed through the following reaction scheme:

$$Pb \longrightarrow Pb(I)_{ad} + e^- \quad (4)$$

$$2\,Pb(I)_{ad} \longrightarrow (Pb(I))_{2,ad} \quad (5)$$

$$(Pb(I))_{2,ad} \longrightarrow 2\,Pb^{2+}_{aq} + 2\,e^- \quad (6)$$

where the recombination of adsorbed Pb(I) species, that is, Reaction 5 becomes the rate determining step. Therefore, and in agreement with the reaction orders obtained from the experimental data, these authors postulated:

$$Pb + HSO_4^- \longrightarrow (PbHSO_4)_{ad} + e^- \quad (7)$$

while the molecular recombination, Reaction 5, produces a H_2SO_4 molecule

$$2(PbHSO_4)_{ad} \longrightarrow (Pb^{I}.SO_4.Pb^{I})_{ad} + H_2SO_4 \quad (8)$$

yielding a bi-Pb(I) sulphate, which crosses the double layer as a neutral entity with a simple electron transfer. This complex reaction mechanism of Pb dissolution in sulphuric acid can be explained through a controlling surface process in which adsorbed Pb(I) species intervene and combine. Even though the identity of this species was not unambiguously established, there is strong evidence suggesting the formation of intermediates stabilized by combination with either HSO_4^- or SO_4^{2-} ions.

2.2. *Lead electrode passivation*

The passivation of Pb electrodes in H_2SO_4 solutions is closely related to the formation of lead sulphate species on the metal surface, whose kinetics and mechanism have been extensively studied [10–12]. However, the electrochemical processes leading to $PbSO_4$ formation on Pb are not yet completely understood because of discrepancies concerning the influence of certain variables on the global process [11, 13, 14], such as electrode surface preparation [7, 8, 11, 15] and solution hydrodynamics [8, 11].

Studies on Pb electrooxidation employing the rotating ring-disc electrode technique showed that during a potential sweep applied to Pb-disc electrode, soluble Pb(II) species were detected on the ring electrode at potentials corresponding to the initial stages of the active–passive transition of Pb [16, 17]. As the maximum currents at the ring and the disc are not synchronic, the formation of the passive film influences the lead dissolution reaction [16]. The experimental results have led kinetic data being interpreted on the basis of several mechanisms, that can be summarized in four main reaction models [8, 13]:

(i) A dissolution–precipitation reaction model [7, 11] in which $PbSO_4$ nuclei form in the solution near the lead surface, and further growth of the 3D $PbSO_4$ layer occurs through the electrodissolution of Pb and subsequent incorporation of Pb^{2+} soluble species to the growing nuclei. In this case, metal passivation can be attributed to the surface blockage by the formed $PbSO_4$.

(ii) A solid-state reaction model [18], which involves the nucleation and growth of $PbSO_4$ according to either 2D or 3D kinetics [18–20], and finishes when the metal surface is covered by a $PbSO_4$ layer. Further surface layer growth requires transport of Pb^{2+} ions throughout the previously formed $PbSO_4$ crystals.

(iii) A complex reaction model to explain $PbSO_4$ formation, which includes nucleation and growth of $PbSO_4$ as a parallel process with the electrodissolution yielding soluble Pb^{2+} species [13, 21, 22]. This mechanism implies the initial formation of an ionic conducting thin barrier, which allows migration of Pb^{2+}. This idea was first expressed by Pavlov [23] and Pavlov and Popova [24], who demonstrated that the inner section of the $PbSO_4$ layer acts as a selective membrane at positive overpotentials, allowing the flow of Pb^{2+} ions and blocking the access of SO_4^{2-} ions to the interfacial region simultaneously. Subsequent $PbSO_4$ layer growth requires the diffusion of Pb^{2+} ions through the $PbSO_4$ layer and precipitation as $PbSO_4$. The suggestion that the initial $PbSO_4$ layer acts as semipermeable membrane at certain potential regions has been mentioned by several authors [18, 25].

(iv) Varela *et al.* [26, 27] have proposed a complex model, which includes several separate steps that take place at multiple reaction interfaces, as illustrated in Fig. 1. The average rate of the overall anodic reaction expressed as $j(t)$, the apparent current density, involves three contributions:

$$j(t) = j_g(t) + j_d(t) + j_f(t) \quad (9)$$

which stand for instantaneous nucleation and 2D growth of the $PbSO_4$ surface film under charge transfer control, $j_g(t)$, for Pb electrodissolution from the film free metal surface fraction, $j_d(t)$, and for Pb dissolution through this initially formed $PbSO_4$ surface film, $j_f(t)$, respectively. The kinetics of the inner $PbSO_4$ layer formation is governed by an instantaneous nu-

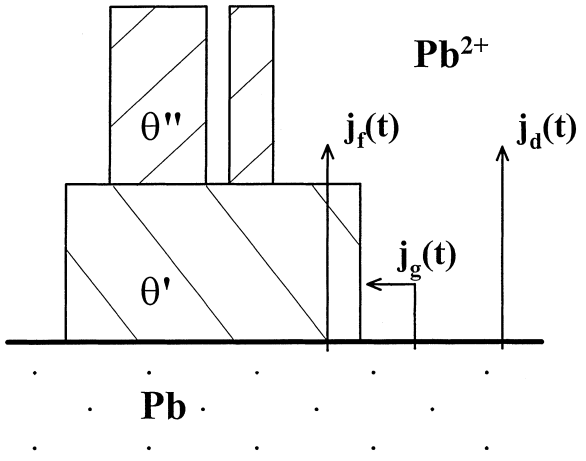

Fig. 1. Scheme of the electrode cross sections during the discharge process. ⊡ Pb; ▨ $PbSO_4$ conducting layer (θ'); ▨ $PbSO_4$ passivation layer (θ''). The different current contributions are indicated.

cleation process followed by 2D growth under charge transfer control [28],

$$j_g(t) = q_g \frac{d\theta'}{dt} = \frac{2\pi n F M_{Su} h_{Su} N_o k^2}{\rho_{Su}} \times t \exp\left(-\frac{\pi N_o M_{Su}^2 k^2}{\rho_{Su}^2} t^2\right) \quad (10)$$

where θ' is the fractional Pb surface coverage by the inner $PbSO_4$ film (Fig. 1), q_g the apparent charge density of this layer, N_o the number of nuclei formed instantaneously, k the average film growth rate constant, and M_{Su}, ρ_{Su} and h_{Su} the molecular weight, the density and the average height of the inner lead sulphate layer, respectively.

The dissolution of Pb^{2+} from the bare lead surface must be proportional to the fraction of the surface not covered by the film $(1 - \theta')$. Thus,

$$j_d(t) = j_d^\circ (1 - \theta') \quad (11)$$

where j_d° stands for the Pb^{2+} electrodissolution current at $\theta' = 0\,(t = 0)$.

Electrode processes described by Equations 10 and 11 are insufficient to account for the observed current transients. Hence, it is proposed that the inner $PbSO_4$ film transmits cations by electromigration in the solid state. These Pb^{2+} cations will enter the electrolyte solution at the outer surface of the film and contribute to the buildup of dissolved Pb^{2+} adjacent to the electrode. The anodic current corresponding to the film transmission is proportional to the film coverage θ', but diminishes by the fractional coverage θ'' of a passivating layer of $PbSO_4$ that precipitates on top of the conductive film $(0 \le \theta'' \le \theta')$;

$$j_f(t) = 2Fk_f(\theta' - \theta'') \quad (12)$$

Once the concentration of dissolved Pb^{2+} reaches the critical supersaturation limit, precipitation of polycrystalline $PbSO_4$ takes place on the outer surface of the conductive inner film,

$$\frac{d\theta''}{dt} = k_p(\theta' - \theta'') \quad (13)$$

This outer passive film does not transmit Pb^{2+} ions and, accordingly, the electrode passivates.

Experiments carried out in the Pb electrooxidation potential region have been fitted satisfactorily using the mechanism given by Equations 9–13. The good agreement between theoretical and experimental data are shown in Fig. 2. Results show that during a transient, the dissolution–precipitation mechanism $j_d(t)$ predominates at short times, whereas the contribution corresponding to the nucleation and growth process $j_g(t)$ becomes important at longer times. Fitted system parameters yielded values of potential-dependent film thickness and kinetic constants. Particularly, the potential dependence of j_d° fulfills a Tafel equation with slope values close to 30 and 120 mV decade^{-1} at low and high overpotentials, respectively. This agrees, in principle, with an initial reversible behaviour of the $Pb \leftrightarrow Pb^{2+} + 2\,e^-$ reaction, which becomes activation controlled with increasing potential. As expected, the value of $(2Fk_f)$, which represents the dissolution of the Pb electrode surface when the conducting $PbSO_4$ layer has already grown, becomes smaller than that obtained through the fitting of j_d°. Nevertheless, as the cation transfer through the film is a slow process, the contribution $j_f(t)$ explains the slow decay of the current exceeding the current peak and represents the main contribution of $j(t)$ for long time polarizations at any anodic potential. Voltammogram computer simulations considered that a potential sweep is the sum of an infinite number of potentials increments and that between successive increments the surface coverage of the Pb electrode remains constant [27].

The formation of Pb(II) soluble species during anodization can be detected using the ring–disc electrode technique, and it was found that the electroreduction charge corresponding to the Pb^{2+} ions reduced at the ring diminishes as the disc potential is shifted more positively [26]. These results

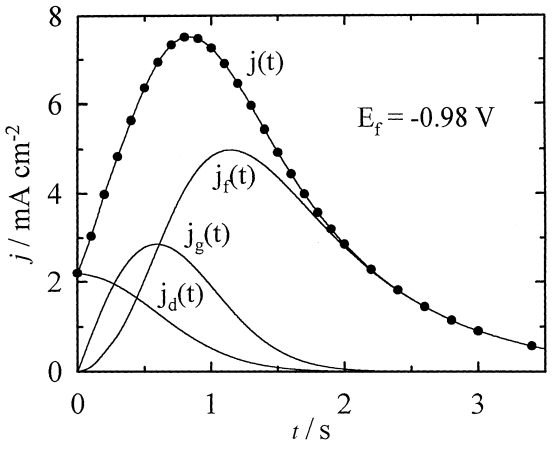

Fig. 2. Comparison of experimental (●) and calculated ($j(t)$) potential step transients. The different anodic current contributions $j_g(t)$, $j_d(t)$, and $j_f(t)$ given by Equations 10–12 are indicated.

agree with data shown in Fig. 2. Likewise, SEM micrographs show that the density of $PbSO_4$ crystals increases with the applied potential, in contrast to the average crystal size [29]. Few and large crystals grow slowly at low potentials under a dissolution–precipitation mechanism, whereas at high anodic overpotentials the nucleation and growth process under charge transfer control, $j_g(t)$, favours the formation of more although smaller $PbSO_4$ cyrstals [29].

According to Pavlov [23, 24], the inner part of the $PbSO_4$ layer acted simultaneously as a permselective membrane for the Pb^{2+} ions, and as a blocking membrane for the access of SO_4^{2-} ions to the interfacial region. This selective permeation determines the accumulation at the inner zone of higher concentration of Pb^{2+} ions than that of SO_4^{2-} [23]. Furthermore, as the formation of the passivating layer θ'' progresses and the pores become narrower (Fig. 1), the Pb^{2+} ion flow is abruptly reduced and, to maintain the electrical neutrality, H^+ ions must migrate from the inner zone into the solution and the solution within the pores becomes more alkaline. This pH gradient is maintained as a dynamic equilibrium between an inward diffusional flow of H^+ from the electrolyte and an outward migrational flow of H^+ from the inner surface layer established by the electric field. At more positive operational potentials, the migrational flow is faster and the internal alkalinization is stronger. Thus, basic compounds of Pb(II) should be formed at high potentials [23, 24, 30, 31].

This reaction mechanism has been recently confirmed by Guo *et al.* [32, 33]. At low overpotentials, the nucleation and growth of the $PbSO_4$ crystals are the controlling steps. However, as the polarization potential increases, the transport of SO_4^{2-} and Pb^{2+} ions through the micropores of the anodic film becomes the dominant process [32]. At long times, the pores become narrower, the anodic reaction progresses controlled by the migration of H^+ and/or OH^- ions, and PbO becomes a stable reaction product as result of the alkalinization of the Pb/$PbSO_4$ interface [32, 33]. Furthermore, Danel and Plichon [16] demonstrated that the lead electrode discharge mechanism remains consistent when the concentration of H_2SO_4 changes, even if the passive layer thickness depends on the solution pH. Likewise, there is spectroscopic evidence confirming that with the increase of H_2SO_4 concentration in solution, the lead sulphate layers passivate the electrode at thinner deposit thickness, growing as a more perfect and dense layer on the metallic surface [34].

2.3. *Lead electrode passive state*

Solid state processes in passive layers on Pb have been extensively studied [10–12, 35]. Pavlov and Popova [24] pointed out that Pb in H_2SO_4 can passivate under two different circumstances: by self-passivation at open circuit and by anodic polarization of the electrode. In both cases, the phenomenon is explained as due to the formation of a dense layer of $PbSO_4$ crystals, with intercrystalline channels too small to allow free movement of Pb^{2+} ions from the metallic surface or of SO_4^{2-} and HSO_4^- ions from the solution. Due to the very low solubility of $PbSO_4$ in H_2SO_4 solutions, the stable film grown on the Pb electrode avoids the current to flow, justifying the wide potential region corresponding to the passive behaviour found for the Pb/$PbSO_4$/H_2SO_4 system. In addition, phenomena of passive material recrystallization, which cause an increase in the size of the intercrystalline spaces, have been mentioned as responsible of the Pb self-activation when the anodic polarization is interrupted [24].

The mechanism of the processes occurring during the anodic polarization of the Pb/$PbSO_4$ electrode can be interpreted taking into account the interrelationships that exist among the electrochemical, diffusion, chemical and crystallization processes [23–25]. While anodic polarization is applied to the electrode, metal dissolution occurs, Pb^{2+} ions react with SO_4^{2-} and $PbSO_4$ is formed on the lead surface. During the film growth, lead sulphate crystals block the metallic surface almost entirely and, taking into account the dielectric properties of $PbSO_4$, the electrochemical process stops at the Pb/$PbSO_4$ interface. In these circumstances, only the metallic surface between $PbSO_4$ crystals remains active and the opposite fluxes of Pb^{2+} and SO_4^{2-} ions occur through the intercrystalline channels. Consequently, the components of the chemical reaction, Pb^{2+} and SO_4^{2-}, are separated by a porous dielectric layer of $PbSO_4$ and the reaction between them continues in the region where both ionic fluxes meet. As the reaction advances, the intercrystalline space decreases progressively and the voluminous SO_4^{2-} ions lose free access to the metallic surface. This fact explains the transformation of the $PbSO_4$ layer into a semipermeable membrane [23, 25], which promotes the existence of an inner region within the passive layer in which $C_{Pb^{2+}} > C_{SO_4^{2-}}$. As the solution must remain electrically neutral, the Pb^{2+} excess charge has to be compensated by water dissociation. Since H^+ ion mobility is several times higher than that of Pb^{2+} ions, H^+ ions migrate from the inner region to the solution and the excess of positive charge is compensated by that of OH^- ions produced by water dissociation. Furthermore, the passive film undergoes an inner alkalinization that favours the formation of basic sulphates, hydroxide and even oxides of Pb(II), which are ordinarily unstable in sulphuric acid solutions.

From X-ray diffraction and electrochemical measurements, Pavlov *et al.* [36, 37] pointed out that the nature of the passive films formed on Pb electrodes in H_2SO_4 solutions can be classified into three distinctive potential regions. The passive layer formed at potentials between -0.95 V and -0.30 V (vs Hg/Hg_2SO_4) consists of $PbSO_4$ crystals. The passive layer produced in the potential range from -0.30 to 0.95 V is composed by $PbSO_4$ and an inner layer that involves several Pb(II) basic compounds, which grow progressively under the initially formed porous

structure of $PbSO_4$. When the potential is more positive than 0.95 V, α-PbO_2 and β-PbO_2 species become the predominating anodic products on the surface. These potential regions agree with the voltammograms of Pb in 5 M H_2SO_4 between $E_{s,c} = -1.30$ V and $E_{s,a} = 1.40$ V including different anodizing times τ at $E_{s,a}$ (Fig. 3). The anodic peak A1 corresponds to $PbSO_4$ formation, whereas cathodic peaks C1 and C2 are related to the electroreduction of $PbSO_4$ and PbO species, respectively. The potential region associated with the Pb(II) to Pb(IV) transition appears poorly defined in the voltammograms. Although at potentials more positive than 0.95 V, the Pb(IV)-oxides become the stable products on the surface, a minimum anodization time (τ_{min}) is required to detect its cathodic electroreduction peak (C3) during the negative-going potential scan. It was found that τ_{min} becomes shorter at higher anodizing potentials ($E_{s,a}$).

The variation in the composition of the corrosion product layer has been confirmed by other authors using X-ray diffraction analysis [38–40], photoelectrochemical measurements [35, 39], *in situ* infrared [41, 42] and laser Raman [38, 39, 41] spectroscopies, and electrochemical microgravimetry with quartz crystal (EQCM) [43].

Lead oxides can be represented by the general formula $PbO_n (1 < n < 2)$ [38, 39, 44]. Two polymorphic species have been identified in the lead corrosion films for both PbO (orthorhombic and tetragonal) and PbO_2 (α or rhombic and β or tetragonal). In some occasions, PbO seems to be amorphous. On the other hand, intermediate oxides such as Pb_3O_4 and Pb_2O_3 were found by Burbank [45], who proposed that these intermediate oxides can be interpreted as an infinitude of possible stoichiometries.

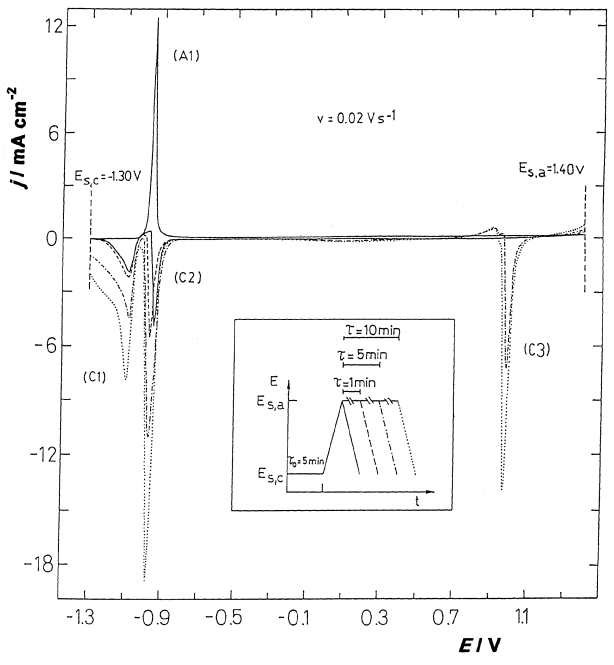

Fig. 3. Influence of anodization time τ at $E_{s,a} = 1.400$ V on voltammograms at $v = 0.020$ V s^{-1} according to the potential program (E/t) indicated in the Figure.

The pH variation within the passive film, can be estimated from thermodynamic values that assure the stability of the basic compounds above mentioned. In this way, it is necessary to calculate the concentration gradient of all the different ions present in the film, because it has been established that, for instance, the pH at which PbO can be formed decreases from 14 to 6.9 when the SO_4^{2-} ions concentration, expressed as pS, changes from 0 to 14 [46]. On the basis of the equilibrium constants for the different possible phases and the electroneutrality principle for the solution, it was suggested recently that under equilibrium conditions, the pH in the PbO inner layer is close to 9, while the activity of Pb^{2+} ions is about $a_{Pb^{2+}} \approx 10^{-5.3}$ and that of SO_4^{2-} ions decreases to $a_{SO_4^{2-}} \approx 10^{-11.2}$ [47]. These values were calculated for the activities in the inner layer and they result relatively independent of the acid concentration in solution, for H_2SO_4 solutions moderately diluted or concentrated, and within the potential region in which PbO is found in the inner portion of passive film.

Considering the different potential regions in which the Pb electrode is covered by passive layers, the broadest zone corresponds to that in which the stable surface film consists of an outer layer of $PbSO_4$ and an inner layer of Pb(II) basic products, mainly PbO [36, 37]. In these conditions, taking into account that $PbSO_4$ behaves as an insulating material [48], studies have mainly been focused on the semiconducting properties of PbO [11].

In situ photoelectrochemical measurements to investigate PbO formation beneath the outer $PbSO_4$ layer were introduced by Pavlov *et al.* [37]. Since lead sulphate is optically transparent to the visible radiation, the subsuperficial corrosion products can be studied without optical interference of this layer. Thus, Pavlov *et al.* found that the PbO grown during lead corrosion in H_2SO_4 yields anodic photocurrents when illuminated with radiation of energy higher than that of the band gap. These photocurrents were characteristic of n-type semiconducting materials and attributed to the photooxidation of tetragonal PbO (*t*-PbO) to a nonstoichiometric oxide such as PbO_n. The mechanism of this process involves photogeneration of holes within the PbO layer. In opposition to these results, Barradas *et al.* [49] concluded from measurements of the band gap energy that the main corrosion product under the $PbSO_4$ layer seems to be orthorhombic PbO (*o*-PbO). Finally, Bullock explained these differences measuring the energy as a function of the corrosion time [38]. The band gap energy shifts from an initial value, close to that of *o*-PbO, towards lower values closer to that of *t*-PbO. In this way, it is explained that *o*-PbO can be initially formed but later *t*-PbO becomes predominant. Moreover, these conclusions were further confirmed by Raman spectroscopy [39] and photoacoustic measurements [50]. Even though Pavlov *et al.* [44] justified that the bandgap energy shift can be assigned to

the film thickness increase and to a change in the stoichiometry of the *t*-PbO layer, they do not disregard the formation of a small amount of *o*-PbO. Currently, the discussion on whether *o*-PbO or *t*-PbO is the first species to grow remains still open.

Furthermore, semiconducting properties of PbO passive layers have been reported as being both n-type and p-type, depending on the aqueous solution chemical composition in which the PbO was grown [51, 52] as well as the film formation potential program [53]. The impedance diagrams recorded in the potential range where a composite Pb(II)-containing sulphate/oxide passive layer is produced, exhibit a complex frequency response, where the insulating behaviour of the $PbSO_4$ layer appears at the lower frequencies [31]. The analysis of high frequency impedance data pointed out that the inner barrier PbO layer behaves as a p-type semiconductor, where the charge carriers concentration decreases slightly as the passive film formation potential is fixed more positively. A Warburg-like diffusion contribution was detected in the intermediate frequency region and that contribution can be attributed to the H^+ ion transport process assisted by the increasing alkalinity of the Pb/film interface as the PbO layer is formed at the inner portion of the surface film [31].

2.4. *Lead*(II)*-species electroreduction (charge process) on lead electrodes*

At relatively low anodization potentials $E_{s,a}$, the electric field through the surface layer and the migrational flow of H^+ maintained by it are insufficient to ensure a significant alkalization, so that the $PbSO_4$ layer continues growing during anodization and, consequently, its electroreduction charge increases according to τ. On the other hand, as $E_{s,a}$ is set more positively, H^+ ions become the main current carriers and the amount of charge associated with the electroreduction of PbO increases with τ, while that of $PbSO_4$ electroreduction remains practically unaltered. This can be confirmed through voltammetric measurements, varying both $E_{s,a}$ and τ [29–31].

For passive films composed by $PbSO_4$ crystals, the cathodic reactions have been studied to examine the effect of organic additives on the nucleation and growth of lead electrocrystallization process [54] and to analyse the difference between the $PbSO_4$ electroreduction process on flat electrodes and that on porous electrodes using the potentiostatic step technique [55]. Data obtained have been discussed mainly according to an instantaneous nucleation and 2D growth process, but a satisfactory fitting to a mathematical model has yet to be done. These electroreduction current transients have also been explained qualitatively with a 3D mechanism [13]. In both cases, experimental data are independent of the hydrodynamics of solution.

The mechanism of $PbSO_4$ electroreduction was studied using the potential sweep technique [56]. Results were interpreted according to a kinetic process in which the main resistance is the mass transport, and a microscopic reaction model developed considering that the reaction driving force is the concentration gradient between the $PbSO_4$ crystal and the Pb electrode surface. Accordingly, experimental data were discussed and potential sweeps simulated in terms of a nucleation and 3D growth process under diffusion control.

Varela *et al.* used combined voltammetry and potentiostatic current transient techniques to study the electroreduction processes of the anodically formed $PbSO_4$ layers at temperatures in the range $0 - 50\,^{\circ}C$ [30 ,57], taking into account that at about $60\,^{\circ}C$ a degradation in operation life of automotive batteries is usually observed [10, 11]. Potentiostatic current transients corresponding to the electroreduction of $PbSO_4$ layers at $-1.10\,V \leq E_f \leq -1.20\,V$ are shown in Fig. 4. The $PbSO_4$ layers were formed at different temperatures by a linear potential scan at $v_a = 0.02\,V\,s^{-1}$ between $E_{s,c} = -1.3\,V$ and $E_{s,a} = E_i = -1.0\,V$. The electroreduction process at E_f was preceded by a potential holding for $\tau = 3$ min at E_i, which is remarkably more negatively located than the potential region of PbO layer formation. These experimental current transients can be satisfactorily reproduced (full traces in Fig. 4) through the expression [30, 57]:

$$j(t) = zFD_j^{1/2}\Delta c_j \pi^{-1/2} t^{-1/2}[1 - \exp(-N_o \pi K_j D_j t)] + zFD_i^{1/2}\Delta c_i \pi^{-1/2} t^{-1/2} \quad (14)$$

where K_j denotes a proportionality constant, $K_j = (8\pi\Delta c_j M_{Su}\rho_{Su}^{-1})^{1/2}$, D_j and Δc_j are the diffusion coefficient and the concentration difference, respectively, of the *j*-species across the Nernst diffusion layer, N_o are the nuclei instantaneously formed, and M_{Su} and ρ_{Su} are the molecular weight and density of $PbSO_4$, respectively. The kinetic data suggest that the electroreduction of $PbSO_4$ layer can be explained with an instantaneous nucleation and 3D growth mechanism under diffusion control. The main contribution implies current control by diffusion of lead ions in the film, the calculated value of $(D_j^{1/2}\Delta c_j)$

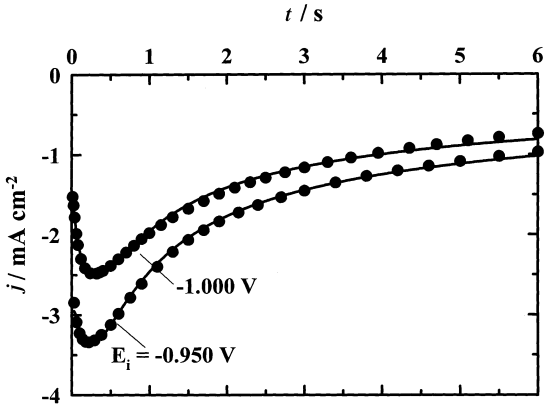

Fig. 4. Fitting of current transient data recorded at $E_f = -1.090$ V after a potential holding at different $E_{s,a} = E_i$ in the $-1.000\,V \leq E_i \leq -0.950\,V$ potential range for $\tau = 3$ min, according to Equation 14 (full traces).

from voltammograms is in accordance with that derived from current transient fit parameters, the diffusion coefficient at 25 °C being in this case about $D_j \approx 3 \times 10^{-11}\,cm^2\,s^{-1}$ and the nuclei instantaneously formed about $8 \times 10^{10}\,cm^{-2}$. In the short-time range, after correction for the electrical double layer discharge, the initial falling current transients obey an instantaneous nucleation and 2D growth under diffusion control. The latter can be associated with the diffusion controlled reversible electroreduction of Pb(II) ions, whose concentration under critical supersaturation condition at 25 °C seems to attain a value of about 2×10^{-6} mol cm $^{-3}$, which is consistent with a diffusion coefficient close to $D_i \approx 10^{-6}$ cm^2 s^{-1}.

Let us consider the following possible consecutive reactions involved in the Pb(II)-sulphate layer electroreduction mechanism:

$$PbSO_4 + H_3O^+ \longrightarrow Pb^{2+} + HSO_4^- + H_2O \quad (15a)$$

$$Pb^{2+} + 2\,e^- \longrightarrow Pb \quad (15b)$$

The set of reactions (15) implies a phase transition process, whose kinetics can be interpreted by a nucleation and 3D growth mechanism under diffusion control, so that H_3O^+/HSO_4^- or Pb^{2+} ions migrate alternately through the $PbSO_4$ layer, and in a fast electron transfer step (Reaction 15(b)) the Pb^{2+} ions are electroreduced on the surface. The calculated activation enthalpy of the diffusion controlling step yields $\Delta H^*_{D_j} = 95.7\,kJ\,mol^{-1}$. This value is in close agreement with that found by Valeriote *et al.* [58] during the oxidation of anodic films on Pb in H_2SO_4 at low temperatures, where the rate-limiting diffusion of ions may be controlled by an activation process involving the partial dehydration of the diffusing ion and/or desorption of interfacial water. On the other hand, for the process occurring during the initial falling current transient, $\Delta H^*_{D_i}$ close to $40.2\,kJ\,mol^{-1}$ was obtained. This value seems to be larger than that expected for an ion diffusion process in solution, but it gives support to the conclusion that can be related to diffusion controlled electroreduction of Pb(II) ions from the supersaturated solution within the pores located between the $PbSO_4$ crystals.

Barradas *et al.* [59] studied the cathodic reduction of PbO using cyclic voltammetry, potentiostatic steps and admittance measurements and they concluded that results can be interpreted using a 3D electrocrystallization theory when PbO is reduced to Pb. It was mentioned, in addition, that at temperatures close to 0 °C, the PbO electroreduction peak splits in two contributions, which were attributed to the reductions of two different faces of a unique material, *o*- and *t*-PbO.

Furthermore, Guo [60] found that the amount of basic sulphates, $PbO \cdot PbSO_4$ and $3PbO \cdot PbSO_4$ formed during potential sweeps can be disregarded in comparison with that of PbO and $PbSO_4$, which are the main constituents of the passive films. The reduction of these compounds appears to be hidden due to an overlapping with an anodic reactivation process, so that $PbO \cdot PbSO_4$ and $3PbO \cdot PbSO_4$ electroreduction taking place at potentials intermediate to those of PbO and $PbSO_4$ electroreduction, cannot practically be observed during potential sweeps. Guo [61] described the kinetic of the PbO electroreduction to Pb according to a 2D process with different nucleation rates, which depend on the reduction overpotential, but included also a slow growth in the perpendicular direction to the electrode surface. On the basis of data analysis using dimensionless representations of the different electrocrystallization models, Guo concluded that the process can be instantaneous or progressive, depending on the value of the applied potential step. Moreover, the transference of reactioning ions throughout the anodic layer was mentioned as another limiting process of the PbO electroreduction reaction, corresponding to the diffusion of OH^- ions throughout the $PbSO_4$ membrane [62].

Varela *et al.* performed a dynamic system analysis to the whole set of data resulting from combined voltammetry and potentiostatic current transient techniques [30, 63, 64]. The kinetics of the electroreduction of PbO layers can be mainly explained in terms of a progressive nucleation and 3D growth mechanism under charge transfer control. In addition, a process under H^+ ion diffusion control has been detected in the short time range. This initial process is related to the electroreduction of Pb(II) ions controlled by the diffusion of H^+ from the outer $PbSO_4$ layer to the inner passive film.

Potentiostatic cathodic current transients of the PbO electroreduction process at $E_f = -0.90$ V are shown in Fig. 5. These transients correspond to PbO layers formed at different $E_{s,a}$, $0.250\ V \le E_{s,a} \le 0.450$ V, for an anodizing time $\tau = 30$ s. According to the kinetic model proposed by Varela *et al.*, these transients can be appropriately described by the expression:

$$j(t) = zF\,k_\perp \theta_i(t)[1 - \theta_i(t)] + P_{D1}\exp(-P_{D2}t) \quad (16)$$

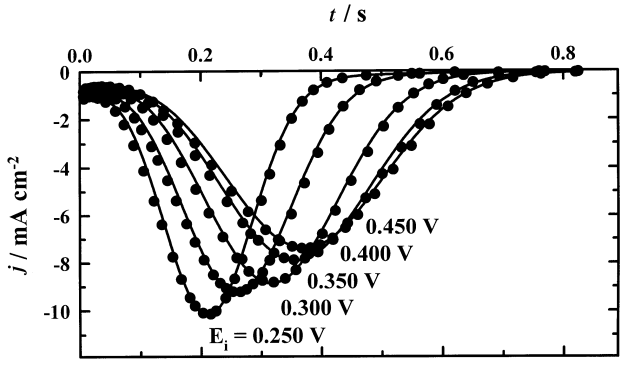

Fig. 5. Fitting of current transient data recorded at $E_f = -1.000$ V after a potential holding at different $E_{s,a}$ in the $0.250\ V \le E_{s,a} \le 0.450$ V potential range for $\tau = 30$ s, according to Equation 16 (full traces).

with

$$\theta_i(t) = \exp\left(-\frac{\pi M_{ox}^2 A k_{\parallel}^2}{3\rho_{ox}^2} t^3\right) \quad (17)$$

where $\theta_i(t)$ denotes the coverage by the PbO species at the inner surface layer, $k_\perp$ and $k_\parallel$ are the rate constants describing crystal growth perpendicular and parallel to the plane surface electrode, respectively, A is the nucleation rate constant, ρ_{ox} the density of the oxide layer, and M_{ox} the PbO molecular weight. In Equation 16, the main term corresponds to the progressive nucleation and 3D growth under charge transfer control process [65], whereas the second term, which predominates only at very short times, is related to the instantaneous nucleation and 2D growth process under diffusion control (P_{D1} and P_{D2}) [63, 64].

Figure 5 also illustrates the good agreement between the experimental and calculated data. The potential E_f was chosen to allow the separation of the electroreduction process of the inner PbO layer from that corresponding to the $PbSO_4$ species, which takes place when $E_f \leq -1.05\,V$. The electroreduction charge Q_{PbO} determined from the current transients increases with τ according to

$$\log Q_{PbO} = -0.5 + 0.5 \log \tau \quad (18)$$

However, at constant τ, Q_{PbO} remains independent of E_f, at least for E_f values within the potential range of the voltammetric peak corresponding to the PbO electroreduction, that is, $-0.82\,V \leq E_f \leq -1.02\,V$. The relationship given in Equation 18 agrees with that obtained from voltammetric electroreduction peak data where it was found that the slope $(\partial \log Q_{PbO}/\partial \log \tau) = 0.5$ is a constant for anodizing potentials $E_{s,a}$ set in the $0.0\,V \leq E_{s,a} \leq 0.6\,V$ range. The values of the model parameters for different E_f and τ, corresponding to $E_{s,a} = 0.40\,V$, can be obtained from the following relationships:

$$\log k_\perp = -12.19 - 8.34\,E_f - 0.101 \log \tau \quad (19)$$

$$\log(A k_{\parallel}^2/\rho_{ox}^2) = -25.94 - 25.10\,E_f - 1.82 \log \tau \quad (20)$$

These relationships yield slopes $[(\partial E_f/\partial \log k_\perp)]_\tau = -0.120\,V\ decade^{-1}$ and $[(\partial E_f/\partial \log(A k_{\parallel}^2/\rho_{ox}^2)]_\tau = 0.040\,V\ decade^{-1}$, values in agreement with those reported previously [63, 64]. Moreover, rate constants of the main current contribution fit an Arrhenius-type behaviour [63]. Results suggest that the thermal increase in the crystal growth perpendicular to the plane surface is about twice that in the parallel direction. Likewise, the activation enthalpy includes two contributions, one related to an ordinary chemical reaction and the other to the reversible electrochemical reaction taking place at the inner portion of the passive film structure [63].

Furthermore, the charge density comprised in the case of the instantaneous nucleation and 2D growth process under diffusion control is given by the P_{D1}/P_{D2} ratio in the second term of Equation 16 [30]. This charge density, which is associated with the small current contribution at short PbO electroreduction times, seems to be practically constant and it involves less than 10% of the whole electroreduction charge. During the previous anodic polarization of Pb electrode, the local pH increases due to the decrease of the concentration of SO_4^{2-} ions and the increase of the concentration of Pb^{2+} at the inner portion of the passive film. When polarization turns into negative values during the charge stage, the Pb^{2+} ion concentration decreases abruptly and, in order to maintain the electroneutrality of the solution in pores, H^+ ions migrate from the solution into the pore and combine with OH^- ions generated during PbO electroreduction. Thus, the initial cathodic current decay can be related to the electroreduction of Pb(II) ions controlled by the diffusion of either OH^- to the solution bulk or H^+ to the inner layer of the passive film.

To achieve a simulation of the electrode response to a cathodic potential sweep, it is necessary to describe the current density, j, and the surface coverage, θ_i, in terms of the dependent variables E and t for any given transient. As the second term of the current density in Equation 16 makes only a small contribution to the whole faradaic charge, for the sake of simplicity it can be neglected in the voltammetric simulations. Thus, the use of Equations 17, 19 and 20 combined with the first term of Equation 16 allows the complete description of voltammograms. The method has been described in detail elsewhere [27, 64, 66]. Simulated cathodic voltammograms after different previous anodizing times τ at $E_{s,a}$ exhibit identical trends to the experimental ones. The apparent cathodic charge density of the simulated voltammograms increases according to τ following Equation 18 closely. As the first term in Equation 16 comprises the main current contribution, the cathodic charge involved in the electroreduction of PbO layers can be approximated by [30]:

$$Q_{PbO} \approx 0.18(zF\,k_\perp)\left(\frac{\pi M_{ox}^2 A k_{\parallel}^2}{3\rho_{ox}^2}\right)^{-1/3} \quad (21)$$

and hence,

$$\log Q_{PbO} \approx \log 0.18 + \log(zF\,k_\perp) - (1/3)\log\left(\frac{\pi M_{ox}^2 A k_{\parallel}^2}{3\rho_{ox}^2}\right) \quad (22)$$

Thus, the parametric functionalities of kinetic rate constants given by Equations 19 and 20 approach the values predicted by the well-established reaction model, according to Equations 18 and 22.

Data analysis allows the conclusion that the reactions involved in the discharge/charge processes of the Pb electrode in H_2SO_4 can be interpreted in terms of electrocrystallization mechanisms. Thus, the electrochemical process related to the discharge of Pb electrode can be explained through a complex mechanism that includes a nucleation and 2D growth under charge-transfer process in parallel with a

dissolution–precipitation one. On the other hand, the electroreduction of the $PbSO_4$ layer during the charge process involves mainly an instantaneous nucleation and 3D growth mechanism under diffusion control.

Furthermore, as the internal alkalization of the $PbSO_4$ layer promotes the formation of basic Pb(II) compounds, it was established that the rate determining step of the slow PbO layer growth is a mass transfer process: the migration of H^+/OH^- ions through the anodic layer. During the electroreduction of the PbO film, however, the H^+/OH^- diffusion controlled process represents less than 10% of the whole electroreduction charge. Likewise, the main electroreduction contribution corresponds to a 3D progressive nucleation with charge transfer controlled growth process.

3. Lead dioxide (positive) electrode

3.1. *Anodic formation* (*charge process*) *of lead dioxide*

The performance of lead–acid battery positive plates depends on grid corrosion processes as well as on the softening and shedding of PbO_2 electrode active material [67, 68]. Progressive transformations taking place in the electrode material during discharge/charge cycles are closely related to the growth of lead sulphate and lead dioxide crystals [69, 70]. Accordingly, changes in phase composition of the surface layers generated in the lead dioxide potential region depends on the electrode potential and on the amount of charge involved during potential cycling of the active material. Rotating ring–disc measurements have demonstrated that both Pb(II) and Pb(IV) soluble species are produced during the electroformation and electroreduction of PbO_2 on Pb electrodes [71, 72]. Data obtained from photoelectrochemical experiments led to the conclusion that the surface layers formed during the charge process at high positive potentials contain non-stoichiometric lead oxides PbO_n $(1 < n < 2)$ besides $PbSO_4$, *t*-PbO and PbO_2 species [23, 73]. The oxidation process of the active material seems to be assisted by the transport of O^{2-} ions across the outer layer, whereas the oxygen evolution reaction takes place mainly at the PbO_2/electrolyte interface [74, 75].

In spite of the large amount of research concerning the electroformation of PbO_2 the electrode reaction mechanism has not been established unequivocally [76–84]. Probably, over narrow potential regions close to the $PbO_2/PbSO_4$ equilibrium potential (1.70 V vs HESS in 4.2 M H_2SO_4 [85], which corresponds to about 1.00 Vvs HgSE), the rate determining step of the growth process of α-PbO_2 and β-PbO_2 species is the diffusion of Pb(II) ions across the inner layer and Pb(IV) ions through the α-$PbO_2/PbSO_4$ interface, respectively [76, 77]. At more positive potentials, however, a detailed knowledge of the reaction pathway associated with the nucleation of the new phase and the concomitant oxygen evolution is still open to discussion.

Different models related to the mechanism of nucleation and growth process of PbO_2 films on preanodized Pb electrodes have been developed [78–83]. Fleischmann *et al.* [78] studied the mechanism of the electrooxidation of $PbSO_4$ potentiostatically formed on Pb electrodeposited onto Cu substrate, where $PbSO_4$ oxidation seems to be controlled by nucleation and 3D crystal growth. Casson *et al.* [79] using Pb electrodeposited onto lead electrodes, found that the current–time response under potentiostatic control after the first potentiodynamic cycle involved two processes: an instantaneous nucleation and the single layer growth of PbO_2 followed by the conversion of the remaining layer of $PbSO_4$ in a more extensive layer. Hampson *et al.* [80] investigated the electrooxidation mechanism for the cycled Pb electrode and proposed an instantaneous nucleation and 2D growth process. Hämeenoja *et al.* [81] demonstrated that it can be well interpreted as a progressive nucleation and 3D growth process with some 2D character. Potentiostatic polarization measurements of the growth of PbO_2 layers on Pb electrodes carried out by Pohl *et al.* [82], showed that during the initial period a closed PbO_2 layer is formed, and subsequently the phase growth takes place according to a parabolic rate law. Wang *et al.* [83] suggested that for the uncycled Pb electrode the electroformation PbO_2 obeys the laws of 2D instantaneous nucleation and growth.

Vilche *et al.* [84] studied the potentiostatic electroformation of PbO_2 on uncycled Pb electrodes; this process was mainly modelled according to an instantaneous nucleation and 2D growth mechanism under charge transfer control associated with the β-PbO_2 phase generation $(j_\beta(t))$, while a α-PbO_2 monolayer growth takes place, probably, on the underlying PbO layer according to a 2D nucleation and 2D growth mechanism $(j_\alpha(t))$. A third contribution is the oxygen evolution $(j_o(t))$, which starts on the $PbSO_4/\beta$-PbO_2 surface, and continues on the β-PbO_2 layer at prolonged polarization times. Accordingly, the kinetics of the electrooxidation at constant potentials located in the region where the Pb electrode is covered by a surface layer whose composition approaches $PbSO_4/PbO_n$ $(1 \leq n \leq 2)$ can be satisfactorily reproduced (Fig. 6), through the following equation:

$$j(t) = j_\alpha(t) + j_\beta(t) + j_o(t) \tag{23}$$

$$j_\alpha(t) = q_{\mathrm{mon},\alpha}\,\pi\,k_\alpha\,D_\alpha\,N^*_{o\alpha}\,\exp\left(-\pi\,k_\alpha\,D_\alpha\,N^*_{o\alpha}t\right) \tag{24}$$

$$j_\beta(t) = (k_\beta + k_{o,e})\,2\,\pi\,z\,F\,M_\beta\,h_\beta\,k_\beta\,N_{o\beta}(\rho_\beta)^{-1} \times t\,\exp\left[-\pi\,M_\beta^2\,k_\beta\,N_{o\beta}(\rho_\beta)^{-2}\,t^2\right] \tag{25}$$

$$j_o(t) = z\,F\,k_{o,t}\left(1 - \exp\left[-\pi\,M_\beta^2\,k_\beta\,N_{o\beta}\,(\rho_\beta)^{-2}\,t^2\right]\right) \tag{26}$$

where $k_\alpha = (8\,\pi\,C_\alpha V_{m\alpha})^{1/2}$, D_α denotes the diffusion coefficient of the mobile species of concentration C_α within the pores, $V_{m\alpha}$ the molar volume, $N^*_{o\alpha}$ the number of active centres, and $q_{\mathrm{mon},\alpha}$ the monolayer charge density of α-PbO_2. Furthermore, $N_{o\beta}$ are the nuclei instantaneously formed, M_β and ρ_β the molecular weight and density, and h_β the thickness of β-PbO_2 film, k_β is the rate constant describing crystal

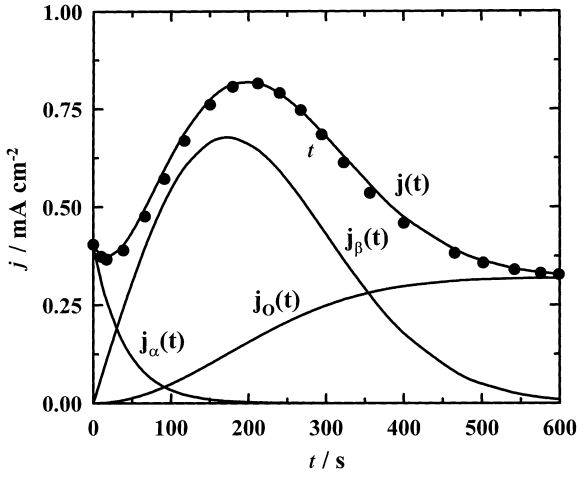

Fig. 6. Comparison of experimental (●) and calculated ($j(t)$) potential step transients. The different anodic current contributions $j_\alpha(t)$, $j_\beta(t)$ and $j_o(t)$ given by Equations 24–26 are indicated. $E_{s,a} = 1.400$ V.

growth parallel to the substrate, and $k_{o,e}$ and $k_{o,t}$ are rate constants for oxygen evolution at the edges and at the top surfaces of β-PbO_2 growth centres, respectively.

In comparison with the current transient during anodization at $E_{s,a} = 1.40$ V shown in Fig. 6, at lower anodic overpotentials for PbO_2 formation the minimum and maximum currents are shifted towards longer anodizing times. The impedance diagrams measured during the electroformation of PbO_2 layers at $E_{s,a} = 1.15$ V at polarization times τ corresponding to the minimum, maximum and stationary current values reveal the presence of at least one additional time constant at short τ (Fig. 7), which disappears with prolonged anodizing time. These results confirm the changes of passive layer morphology occurring at short anodizing times probably due to the consumption of the $PbSO_4$ insulating layer and the simultaneous formation of a more conducting PbO_2 layer.

3.2. *Electroreduction (discharge process) of PbO_2*

The electroreduction of PbO_2 in H_2SO_4 during the discharge process of the positive electrode of lead–acid battery takes place via the following reaction:

$$PbO_2 + 4\,H^+ + SO_4^{2-} + 2\,e^- \longrightarrow PbSO_4 + 2\,H_2O \quad (27)$$

Since the 1970s, research has been focused on the reduction of porous PbO_2 active material on lead and the electroreduction of deposited β-PbO_2 or α-PbO_2 film on an inert substrate [86, 87]. Depending upon

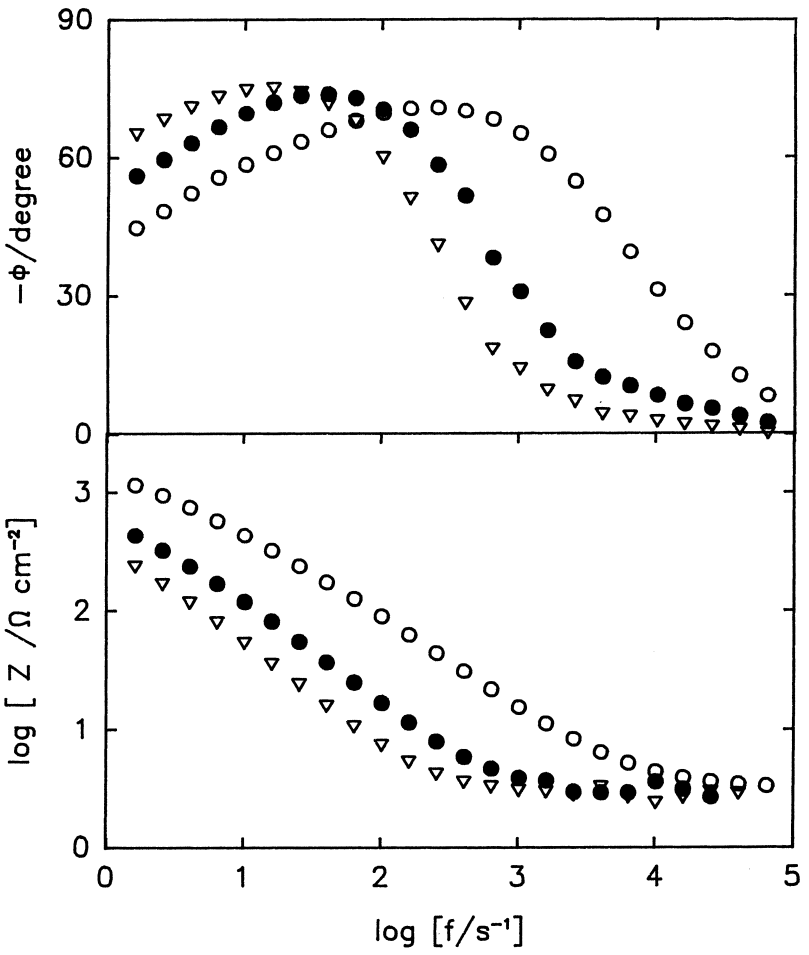

Fig. 7. Bode plots measured after different anodizing times at $E_{s,a} = 1.150$ V. τ: (○) 3, (●) 23 and (▽) 60 min.

the time and potential of anodic treatment, both polymorphs may be present in the surface film [14, 25]. Through TEM observations it was established that the lead-acid battery PbO_2 active crystals have a nonhomogeneous mass distribution and contain some defects in their crystal lattice [88, 89]. From electron diffraction analysis of the active mass agglomerates and individual crystals it was determined that β-PbO_2 is formed in the long and needle-like crystals, while α-PbO_2 is presented in the short and slab-like crystals often with a nonuniform shape [89, 90].

The photocurrent method has proved to be a sensitive *in situ* technique for characterizing photoactive lead oxides in the anodic films on lead formed at 0.4−0.9 V vs Hg/Hg_2SO_4 in H_2SO_4 [35, 38, 44, 91]. *t*-PbO, *o*-PbO and PbO_n $(1 < n < 1.4)$ have been found to be photoactive semiconductors, while PbO_2 and PbO_n and $(1.4 < n < 2)$ are photoinactive conductors [73, 92]. In this context, the overall reaction on discharge can be represented by

$$PbO_2 + 2(2-n)\,H^+ + 2(2-n)e^- \longrightarrow PbO_n + (2-n)\,H_2O \quad (28)$$

$$PbO_n + (2n-1)\,H^+ + HSO_4^- + 2(n-1)e^- \longrightarrow PbSO_4 + n\,H_2O \quad (29)$$

The discharge reaction of positive plates was also investigated using rotating ring-disc electrode technique. The presence of soluble Pb(IV) [71] and Pb(II) [93] species during the charge and discharge processes, respectively, suggested that the electroreduction of PbO_2 can occur through a dissolution–precipitation mechanism. Another possible mechanism for the formation of the reticulate structure of $PbSO_4$ seems to be a solid-state electroreduction process. Hampson *et al.* [87, 94] found that the electrocrystallization of this $PbSO_4$ on Pb electrode takes place via progressive nucleation and 2D growth.

Figure 8 shows the dependence on $E_{s,a}$ of the charge density involved in peaks C1, C2 and C3 recorded at $v = 0.04\,V\,s^{-1}$ for $E_{s,a}$ set within the potential range $-1.00\,V \le E_{s,a} \le 1.50\,V$, for different anodizing times (τ) at $E_{s,a}$. The apparent charge density of peak C2 (q_{C2}) increases linearly with the potential $E_{s,a}$. The charge density of peak C1 (q_{C1}), remains approximately constant when $E_{s,a} < 1.00\,V$ and increases with $E_{s,a}$ according to a linear relationship for $E_{s,a} > 1.00\,V$. The increase of q_{C1} is in good agreement with the increase of q_{C3} as $E_{s,a}$ is set more positively (Fig. 7(b)). It is noteworthy that q_{C3} attains a practically constant value in the cathodic voltammograms when the previous anodizing time at $E_{s,a}$ exceeds about 20 min. These results suggest that the generation of Pb(IV) species is accompained by the simultaneous formation of Pb(II) basic compounds, and that the PbO_2 layer is totally electroreduced to $PbSO_4$ species without affecting the PbO electroreduction mechanism.

To study the voltammetric electroreduction of PbO_2 layer in the potential range of the cathodic peak

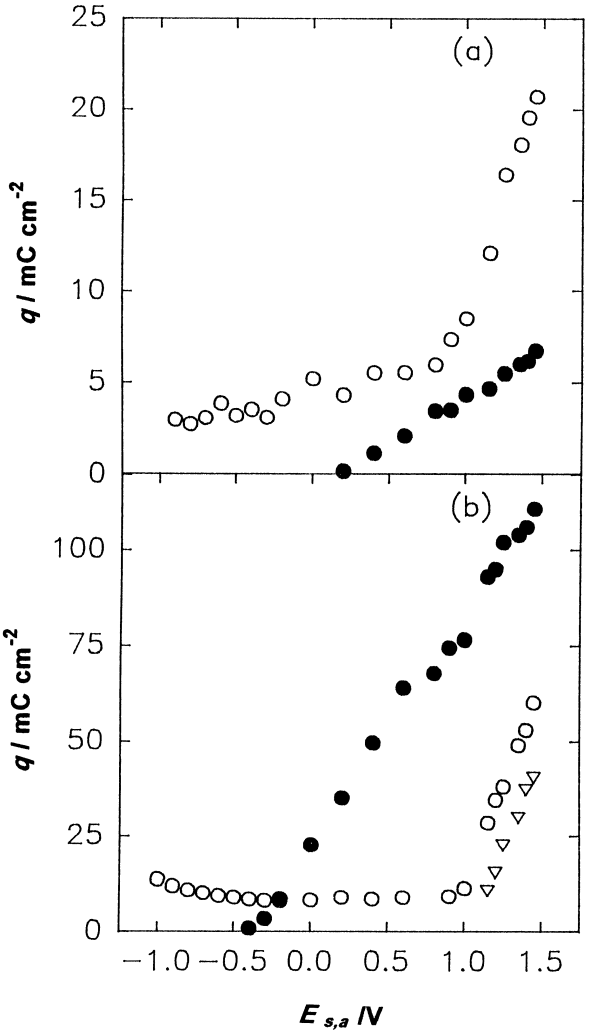

Fig. 8. Dependence of cathodic charge density on $E_{s,a}$ at $v_c = 0.04\,V\,s^{-1}$ for different anodizing times: (a) $\tau = 0$; (b) $\tau = 60$ min. Key for (a) and (b): (○) C1, (●) C2 and (▽) C3.

C3, the previous formation of these layers was carried out by a lineal potential sweep at $v_a = 0.04\,V\,s^{-1}$ up to $E_{s,a} = 1.40\,V$, and then the anodic surface product allowed to grow at $E_{s,a}$ for $\tau = 10$ min. From the potentiodynamic reverse scan at different v_c, the height of current peak C3 ($j_{p,C3}$) exhibits a linear $(j_{p,C3})$ against $v_c^{1/2}$ relationship, whose extrapolation to $v_c \to 0$ yields nearly $(j_{p,C3}) \approx 0$ (Fig. 9(a)). Similar results can be derived independently of both anodic scan rate and hydrodynamic conditions.

This suggests that the electroreduction of PbO_2 taking place in the potential region of peak C3 can be considered as a solid-phase diffusion controlled process. The corresponding q_{C3} against $v_c^{-1/2}$ plot obeys a linear relationship whose extrapolation to $v_c \to 0$ approaches a voltammetric charge density of about $(q_{C3}) \approx 26\,mC\,cm^{-2}$ (Fig. 9(b)). This value is in satisfactory agreement with that determined in potentiostatic cathodic current transient experiments, preceded by an anodizing time $\tau = 10$ min at $E_{s,a} = 1.40\,V$, when the electroreduction process is performed by applying a potential step to $E_f = 0.80\,V$, which yielded $q = 27 \pm 2\,mC\,cm^{-2}$.

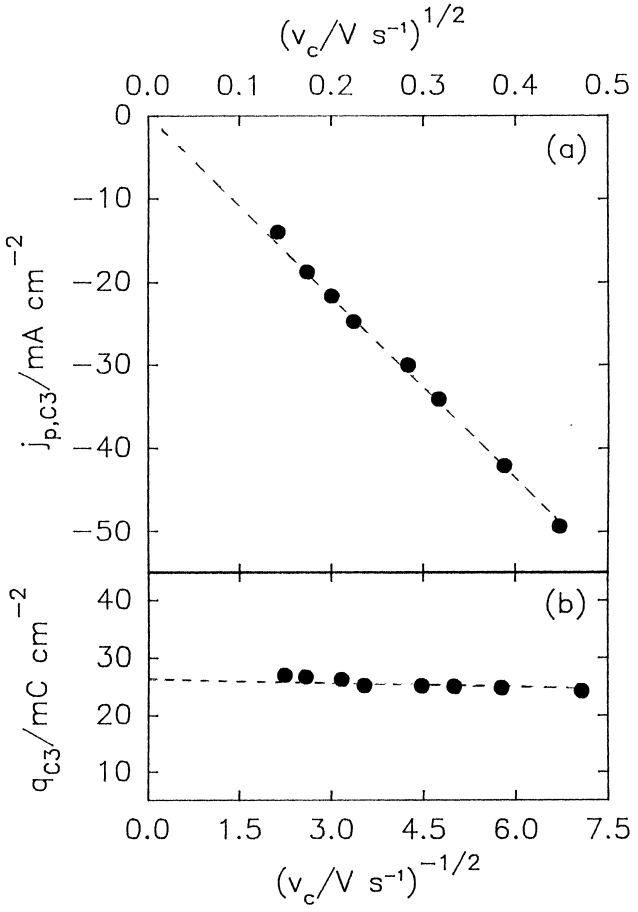

Fig. 9. Dependence of $j_{p,C3}$ on $v_c^{1/2}$ and of $q_{C,3}$ on $v_c^{-1/2}$. $v_a = 0.04$ V s^{-1}; $E_{s,a} = 1.40$ V; $\tau = 10$ min.

4. Conclusions

The kinetics of the charge/discharge electrochemical reactions of lead and lead dioxide electrodes in sulphuric acid solutions were investigated using different potential perturbing and spectroscopic techniques. Dissolution–precipitation mechanisms, electrocrystallization theories and properties of the surface films have been used by several authors to interprete the experimental results.

Successful nucleation and growth models have been developed in order to explain the electrooxidation of Pb and the posterior electroreduction of the surface anodic products, $PbSO_4$ and PbO, reactions that correspond to highly irreversible processes. The formation of Pb(II)-containing compounds within the passive-state potential range, however, has been traditionally described only qualitatively and more complete models that account for the amount of charge passing through the electrode during the passive state were developed only in the last years.

For the PbO_2 electrode it has been found that the discharge/charge processes can be mainly explained through solid-state reaction models. The prenucleation surface conditions, however, determine the electrocrystallization mechanism during anodic polarization. The PbO_2 electroreduction has received considerably less attention. The discharge products of the positive electrode appear to be of an heterogeneous nature. The presence of soluble Pb(II) and/or Pb(IV) species suggests that, at least, one dissolution step is involved in the electroreduction mechanism of PbO_2.

Acknowledgements

This research project was financially supported by the Consejo Nacional de Investigaciones Científicas y Técnicas, the Comisión de Investigaciones Científicas de la Provincia de Buenos Aires, and the Fundación Antorchas. Part of the equipment used in the present work was provided by the DAAD and the Alexander von Humboldt Stiftung.

References

[1] G. Planté, *Compt. Rend.* **49** (1859) 402.
[2] A. Tribe and J. H. Gladstone, *Nature* **25** (1882) 221.
[3] V. Danel and V. Plichon, *Electrochim. Acta* **27** (1982) 771.
[4] J. Garche, P. J. Mitchell and N. H. Hampson, *J. Appl. Electrochem.* **14** (1984) 97.
[5] N. A. Hampson, C. Lazarides, G. M. Bulman and C. Knowles, in *Power Sources* (J. Thompson, ed.) Academic Press, London, **8** (1981) 621.
[6] A. N. Fleming and J. A. Harrison, in 'The Electrochemistry of Lead' (edited by A. T. Kuhn), Academic Press, London/New York (1979).
[7] G. Archdale and J. A. Harrison, *J. Electroanal. Chem.* **34** (1972) 21; *ibid.* **39** (1972) 357.
[8] L. M. Baugh, K. L. Bladen and F. L. Tye, *J. Electroanal. Chem.* **145** (1983) 355.
[9] N. A. Hampson and J. B. Lakeman, *J. Power Sources* **4** (1979) 21.
[10] H. Bode, in 'Lead–Acid Batteries', J. Wiley & Sons, New York (1977).
[11] K. R. Bullock and D. Pavlov (eds.), in 'Advances in Lead–Acid Batteries', The Electrochemical Society, Pennington, NJ (1984).
[12] T. F. Sharpe, in 'Encyclopedia of Electrochemistry of the Elements', Vol. 1 (edited by A. J. Bard), Marcel Dekker, New York (1973), p. 235.
[13] A. N. Fleming and J. A. Harrison, *Electrochim. Acta* **21** (1976) 905.
[14] D. Pavlov and N. Iordanov, *J. Electrochem. Soc.* **117** (1970) 1103.
[15] S. Fletcher and D. B. Matthews, *J. Appl. Electrochem.* **11** (1981) 11; *ibid.* **11** (1981) 23.
[16] V. Danel and V. Plichon, *Electrochim. Acta* **28** (1983) 781, *ibid.* **28** (1983) 785.
[17] T. Laitinen, B. Monahov, K. Salmi and G. Sundholm, *Electrochim. Acta* **36** (1991) 953.
[18] N. A. Hampson and J. B. Lakeman, *J. Electroanal. Chem.* **107** (1980) 177.
[19] R. D. Armstrong and J. A. Harrison, *J. Electrochem. Soc.* **116** (1969) 328.
[20] N. A. Hampson and J. B. Lakeman, *J. Appl. Electrochem.* **9** (1979) 403.
[21] S. B. Hall and G. A. Wright, *Corros. Sci.* **31** (1990) 709.
[22] C. V. D'Alkaine and J. M. Cordeiro, in ref. **[11]**, p. 190.
[23] D. Pavlov, *Electrochim. Acta* **13** (1968) 2051; *ibid.* **23** (1978) 845.
[24] D. Pavlov and R. Popova, *ibid.* **15** (1970) 1483.
[25] P. Ruetschi, *J. Electrochem. Soc.* **120** (1973) 331.
[26] F. E. Varela, M. E. Vela, J. R. Vilche and A. J. Arvia, *Electrochim. Acta* **38** (1993) 1513.
[27] F. E. Varela, J. R. Vilche and A. J. Arvia, *ibid.* **39** (1994) 401.
[28] J. A. Harrison and H. R. Thirsk, in 'Advances in Electroanalytical Chemistry', Vol. 5 (edited by A. J. Bard), Marcel Dekker, New York (1971), pp. 67–148.
[29] F. E. Varela and J. R. Vilche, *J. Power Sources*, in press.
[30] F. E. Varela, L. M. Gassa and J. R. Vilche, *Electrochim. Acta* **37** (1992) 1119.
[31] *Idem*, *J. Electroanal. Chem.* **353** (1993) 147.

[32] Y. Guo, *J. Electrochem. Soc.* **142** (1995) 3643; *ibid.* **142** (1995) 3378.
[33] Y. Guo, S. Hua, H. Xu and Y. Yang, *J. Electrochem. Soc.* **143** (1996) 1157.
[34] J. A. Bialacki, N. A. Hampson, K. Peters and A. K. Williams, *J. Appl. Electrochem.* **13** (1983) 103.
[35] J. S. Buchanan and L. M. Peter, *Electrochim. Acta* **33** (1988) 127.
[36] D. Pavlov, C. N. Poulieff, E. Klaja and N. Iordanov, *J. Electrochem. Soc.* **116** (1969) 316.
[37] D. Pavlov, S. Zanova and G. Papazov, *ibid.* **124** (1977) 1522.
[38] K. R. Bullock, *J. Electroanal. Chem* **222** (1987) 347.
[39] K. R. Bullock, G. M. Trischan and R. G. Burrow, *J. Electrochem. Soc.* **130** (1983) 1283.
[40] Y. Guo, J. Chen and L. Li, *ibid.* **139** (1992) L99.
[41] R. J. Thibeau, C. W. Brown, A. Z. Goldfarb and R. Heidersbach, *J. Electrochem. Soc.* **127** (1980) 37.
[42] G. L. J. Trettenhahn, G. E. Nauer and A. Neckel, *Ber. Bunsenges. Phys. Chem.* **97** (1993) 422.
[43] C. Wei and K. Rajeshwar, *J. Electrochem. Soc.* **140** (1993) L128.
[44] M. Dimitrov, K. Kochev and D. Pavlov, *J. Electroanal. Chem.* **183** (1985) 145.
[45] J. Burbank, *J. Electrochem. Soc.* **106** (1959) 369.
[46] K. R. Bullock, *ibid.* **127** (1980) 662.
[47] Y. Guo, *ibid.* **139** (1992) 2114.
[48] E. W. Washburn (ed.), in 'International Critical Tables of Numerical Data: Physics, Chemistry and Technology', McGraw-Hill, New York (1928).
[49] R. G. Barradas, D. S. Nadezhdin, J. B. Webb, A. B. Roth and D. F. Williams, *J. Electroanal. Chem.* **126** (1981) 273.
[50] G. H. Brilmyer, in ref. [**11**], p. 142.
[51] L. Heijne, *J. Phys. Chem. Solids* **22** (1961) 207.
[52] K. L. Hardee and A. J. Bard, *J. Electrochem. Soc.* **124** (1977) 215.
[53] S. Fletcher and D. B. Matthews, *J. Electroanal. Chem.* **126** (1981) 131.
[54] M. P. J. Brennan and N. A. Hampson, *ibid.* **52** (1974) 1.
[55] N. A. Hampson and J. B. Lakeman, *ibid.* **108** (1980) 347.
[56] K. Kanamura and Z. Takehara, *J. Electrochem. Soc.* **139** (1992) 345.
[57] F. E. Varela, L. M. Gassa and J. R. Vilche, *J. Appl. Electrochem.* **25** (1995) 358.
[58] E. M. L. Valeriote and L. D. Gallop, *J. Electrochem. Soc.* **124** (1977) 370; *ibid.* **124** (1977) 380.
[59] R. G. Barradas and D. S. Nadezhdin, *Can. J. Chem.* **62** (1984) 596.
[60] Y. Guo, *J. Electrochem. Soc.* **138** (1991) 1222.
[61] *Idem*, *J. Electroanal. Chem.* **317** (1991) 229.
[62] *Idem*, *Electrochim. Acta.* **37** (1992) 495.
[63] F. E. Varela, L. M. Gassa and J. R. Vilche, *J. Appl. Electrochem.* **25** (1995) 364.
[64] F. E. Varela, E. N. Codaro and J. R. Vilche, *Electrochim. Acta* **40** (1995) 1183.
[65] R. D. Armstrong, M. Fleischmann and H. R. Thirsk, *J. Electroanal. Chem.* **11** (1966) 208.
[66] R. G. Barradas, F. C. Benson and S. Fletcher, *J. Electroanal. Chem.* **80** (1977) 305.
[67] W. Hofmann, in 'Lead and Lead Alloys' (edited by G. Vibrans), Springer-Verlag, Berlin (1970).
[68] J. Broadhead and D. H. Collins (Eds.), in 'Lead-Acid Batteries,' *Journal of Power Sources* **2**, Elsevier Sequoia, Switzerland (1977/78).
[69] N. A. Hampson and S. Kelly, in 'Power Sources 8' (edited by J. Thompson), Academic Press, London, (1981) pp. 535–47.
[70] R. R. Nilson, *J. Power Sources* **41** (1993) 1.
[71] M. Skyllas-Kazacos, *J. Electrochem.Soc.* **128** (1981) 817.
[72] T. Laitinen, B. Monahov, K. Salmi and G. Sundholm, *Electrochim. Acta* **36** (1991) 953.
[73] K. R. Bullock and M. A. Butler, *J. Electrochem. Soc.* **133** (1986) 1085.
[74] D. Pavlov and T. Rogachev, *Electrochim. Acta* **23** (1978) 1237.
[75] J. P. Pohl and W. Schendler, *J. Power Sources* **13** (1984) 101.
[76] E. M. L. Valeriote and L. D. Gallop, *J. Electrochem. Soc.* **124** (1977) 370.
[77] D. Pavlov and Z. Dinev, *J. Electrochem. Soc.* **127** (1980) 855.
[78] M. Fleischmann and H. R. Thirks, *Trans. Faraday Soc.* **51** (1955) 71.
[79] P. Casson, N. A. Hampson and K. Peters, *J. Electroanal. Chem.* **83** (1977) 87.
[80] N. A. Hampson, S. Kelly and K. Peters, *J. Appl. ElectroChem.* **10** (1980) 261.
[81] E. Hämeenoja and N. A. Hampson, *J. Appl. Electrochem.* **14** (1984) 449.
[82] T. Laitinen and J. P. Pohl, *Electrochim. Acta* **34** (1989) 377.
[83] J. Wang and G. Wei, *J. Electroanal. Chem.* **390** (1995) 29.
[84] E. N. Codaro and J. R. Vilche, *Electrochim. Acta*, in press.
[85] P. Rüetschi and R. T. Angstadt, *J. Electrochem. Soc.* **111** (1964) 1323.
[86] J. P. Carr and N. A. Hampson, *Chem. Rev.* **72** (1972) 679.
[87] S. R. Ellis, N. A. Hampson, M. C. Ball and F. Wilkinson, *J. Appl. Electrochem.* **16** (1986) 159.
[88] P. T. Moseley, J. L. Hutchinson and M. A. M. Bourke, *J. Electrochem. Soc.* **129** (1982) 876.
[89] D. Pavlov and E. Bashtavelova, *J. Electrochem. Soc.* **133** (1986) 241.
[90] P. Casson, I. Balkanov and P. Rachev, *ibid.* **134** (1987) 2390.
[91] J. Han, C. Pu and W. Zhou, *J. Electroanal. Chem.* **368** (1994) 43.
[92] W. Cai, Y. Wan, H. Liu and W. Zhou, *J. Electroanal. Chem.* **387** (1995) 95.
[93] Z. Takehara and K. Kanamura, *Electrochim. Acta* **29** (1984) 1643.
[94] N. A. Hampson, S. Webster, P. J. Mitchell and J. Dyson, *J. Electrochem. Soc.* **113** (1986) 113.